IRAMP
11(1), Jan 2020, pp. 7-26

ISSN: 2229-39-44

Cyanide Laser-Plasma Spectroscopy in a Flowing Gaseous Mixture

CHRISTOPHER M. HELSTERN, CHRISTIAN G. PARIGGER*

Physics and Astronomy Department, University of Tennessee,
University of Tennessee Space Institute, Center for Laser Applications,
411 B.H. Goethert Parkway, Tullahoma, TN 37388-9700, USA
**Corresponding author E-mail: cparigge@tennessee.edu (C.G. Parigger)*

ABSTRACT: This article communicates measurements of diatomic molecular cyanide (CN) in a flowing gas mixture. The mixture is composed of 1:1 molar carbon dioxide and nitrogen flowing at a rate of 100 mL per minute. The laser plasma is generated with Q-switched IR irradiance that is a few times above the optical breakdown threshold for the mixture. This work reports recorded spatio-temporal spectral maps. Detailed data curation reveals density, temperature profiles from the line-of-sight measurements. In addition, Abel inversion maps serve the purpose of inferences about the expanding shockwave and expanding kernel of the plasma.

PACS Codes: *52.70.-m, 33.20.-t, 52.25Jm, 42.62.Fi*

Keywords: *Plasma diagnostics, molecular spectra, plasma spectroscopy, laser spectroscopy, laser-induced breakdown spectroscopy.*

1. INTRODUCTION

Cyanide (CN) spectra produced from molecular recombination spectra are measured following optical breakdown in gases for time delays of the order of 100 ns after the end of the laser pulse [1]. CN plasma dynamics are observed by using gas mixtures. Applications of cyanide spectroscopy include potential medical and forensic applications [2].

In molecular spectroscopy, the molecular Hamiltonian determines the overall framework of the molecular emissions. The Hamiltonian accounts for electronic, vibrational, and rotational components due to vibrations and rotations associated with molecules. Additionally, the total molecular Hamiltonian contains influences due to molecular nuclei motion and nucleonic spins. This Hamiltonian consists of quantized rotations and vibrations. Spectral lines produced by vibrations and rotations correlate to transitions between quantum numbers associated with vibrations and rotations. The principal idea of a molecular emission is that there is a separate potential energy curve for each electronic state. Quantized vibrations represent splitting of these potentials and rotational splitting of these vibrations occur. Figure 1 shows the plotting of the potentials, V, versus the internuclear separation coordinate R. The potentials shown in Figure 1 are known as Morse potentials, which results from the work of Morse [3]. Electronic transitions, vibrational transitions, and rotational transitions represent the organizational structure of the spectral emission, respectively. Due to vibrational transitions being similar in electronic position, band like structures are formed.

Cyanide (CN) is a diatomic molecule and has two characteristic electronic systems. These two systems are the violet ($B^2\Sigma^+$–$X^2\Sigma^+$, 344–460 nm) and the red ($A^2\Pi$–$X^2\Sigma^+$, 437–1500 nm), where $X^2\Sigma^+$ state represents the ground state [4]. In this notation A, B, and X represent the potential curves, 2 represents the spin of +1/2 (doublet), Σ and Π represent the angular or orbital quantum number l=0, 1 respectively, and + represents the unchanged symmetry

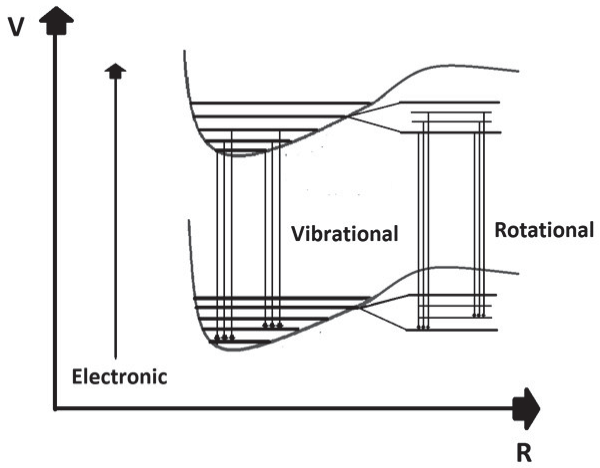

Figure 1: Electronic, vibrational, and rotational spectra as a result of molecular potentials between two electronic levels.

For this work, the CN violet-band Δv=0 system is of interest and these emissions represent vibrational transitions from a higher energy potential ($B^2\Sigma^+$) to the ground state, where Δv=0 means the difference between the vibrational quantum numbers is 0. As shown in Figure 2, if the CN molecule is in a vibrational state in the higher potential represented by vibrational quantum number v=1, it can only transition to the vibrational state in the ground state also represented by quantum number v=1, which would result in the (1,1) band. The CN violet system consists of vibrational bands (0,0), (1,1), (2,2), (3,3) and (4,4), which are 388.34 nm, 387.14 nm, 386.19 nm, 385.47 nm, and 385.09 nm, respectively. In addition to the vibrational states, rotational states exist for the CN violet system which give the system its fine structure.

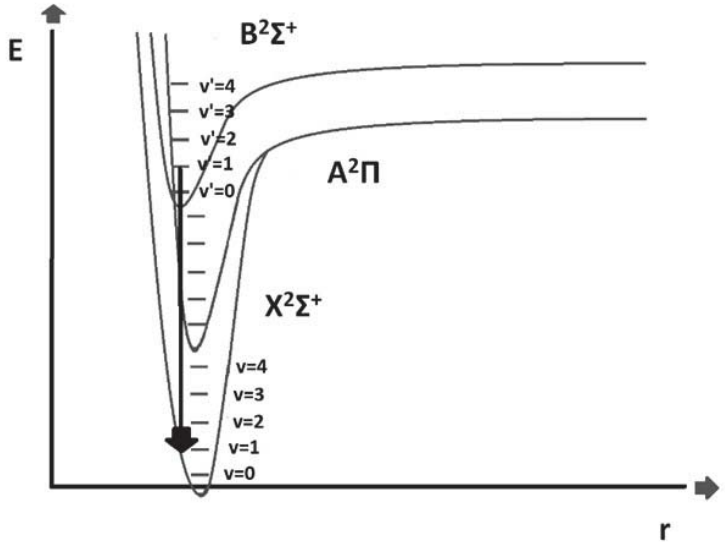

Figure 2: Potential curves of CN.

2. EXPERIMENTAL DETAILS

A set of flowing gas mixture measurements were performed using an experimental setup similar to that of a fixed gas mixture [2], however, the arrangement for laser induced breakdown spectroscopy is included in the next paragraph. A flowmeter (Cole-Parmer Instrument Company model FM112-02ST, USA) was connected to the gas outlet instead of the differential pressure gauge as mentioned in the fixed gas mixture experimental setup. The chamber was supplied with a constant flow of ultrahigh purity N_2 and research-grade CO_2 gas mixture. A flow rate of 100 mL per min of the mixture entered and left the cell, which was monitored by the flowmeter as seen in Figure 3.

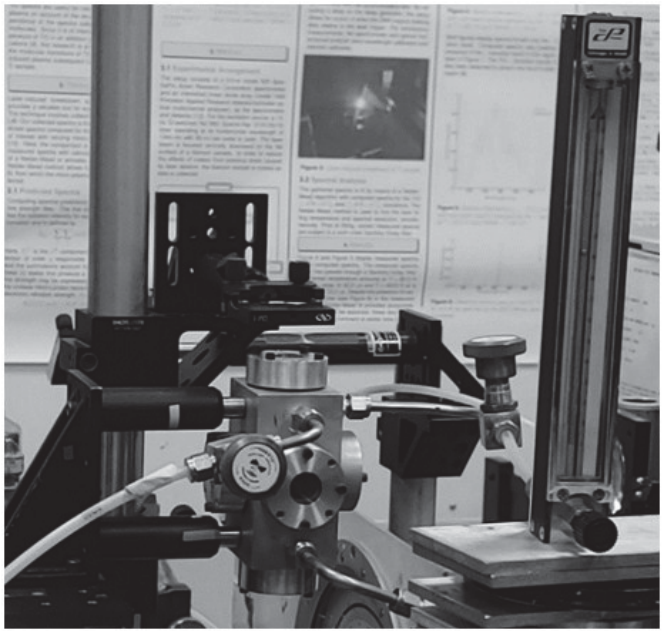

Figure 3: Picture of the gas chamber and flowmeter

Inside the chamber, optical breakdown was created at a rate of 10 Hz using a laser beam focused with f/5 optics from the top or parallel to the slit. Pixels of the ICCD were binned in four-pixel tracks along the slit direction, resulting in the production of 256 spectra for each time delay. Recordings of spectra were performed with and without the Order-Sorting Filter consisting of 100 accumulations collected for 21 time delays at 250 ns steps.

The standard experimental components are used for laser-induced breakdown spectroscopy and have been summarized previously, e.g., see Ref. [2], but are included for completeness. The experimental arrangement consists of a set of components typical for time-resolved, laser-induced optical emission spectroscopy, or nanosecond laser-induced breakdown spectroscopy (LIBS) [5]. Primary instrumentations include a Q-switched Nd: YAG device (Quantel model Q-smart 850) operated at the fundamental wavelength of 1064-nm to produce full-width-at-half-maximum 6-ns laser radiation with an energy of 850 mJ per pulse, a laboratory type Czerny-Turner spectrometer (Jobin Yvon model HR 640) with a 0.64 m focal length and equipped with a 1200 grooves/mm grating, an intensified charge coupled device (Andor Technology model iStar DH334T-25U-03) for recording of temporally and spatially resolved spectral data, a laboratory chamber or cell with inlet and outlet ports together with a vacuum system, electronic components for synchronization, and various optical elements for beam shaping, steering and focusing. Figure 4 displays the principal schematic of the experimental arrangement. The laser beam is focused into the cell through which the 1:1 molar carbon dioxide and nitrogen mixture is flown.

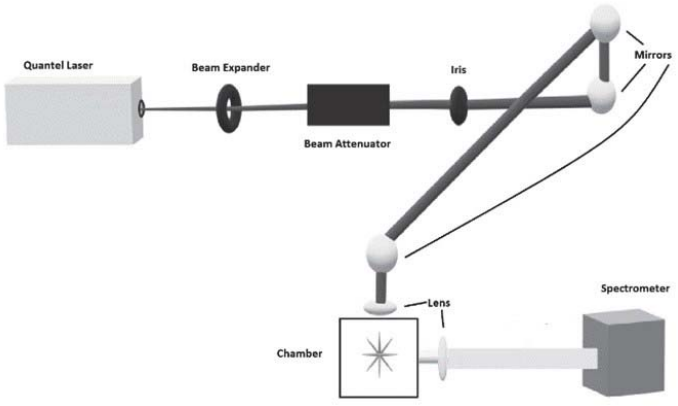

Figure 4: Modular schematic of laser-induced breakdown experiment

For the generation of optical breakdown micro-plasma, a singlet lens (Thorlabs model LA1509-C) is used close to the top entrance window of one arm of the chamber containing the 1:1 CO_2:N_2 gas mixture held at 3.04×10^5 Pascal (Airgas ultra-high purity N_2 and research grade CO_2). For 1:1 imaging of the plasma onto the 100 μm spectrometer slit, a fused silica plano-convex lens (Thorlabs model LA4545) is employed. For the CN experiments, the laser pulse energy is attenuated with beamsplitters and apertures from 850 to 170 mJ/pulse.

3. RESULTS AND DISCUSSION

3.1 Spatially resolved spectra

Optical breakdown was generated inside the chamber at a rate of 10 Hz, with the laser beam focused with f/5 optics from the top, or parallel to the slit. The detector pixels are binned in 4 tracks along the slit direction, resulting in obtaining 256 spectra for each time delay. Recording of measurements consist of 100 accumulations collected for 21 time delays at 250 ns steps. Figures 5 to 7 illustrate recorded spatio-temporal spectra that were recorded along the line-of-sight for a 1:1 molar CO_2:N_2 flowing gas mixture with a flow rate of 100 mL/min, and are accumulated over 100 indiviual laser-plasma events and the CI 193.09 nm atomic carbon line as indentified in previous work [6 – 8]. Similar to the gaseous mixture of fixed volume, the CN violet system $B^2\Sigma^+$–$X^2\Sigma^+$ vibrational bands of (0,0), (1,1), (2,2), (3,3) and (4,4) are clearly visible. Additionally, the overlap of the CI 193.09 nm atomic carbon line in second order and the (2,2) band head is present as in the gaseous mixture of fixed volume. At time delays greater than 2.2 μs, the CI 193.09 nm atomic carbon line in second order appears to dissipate away.

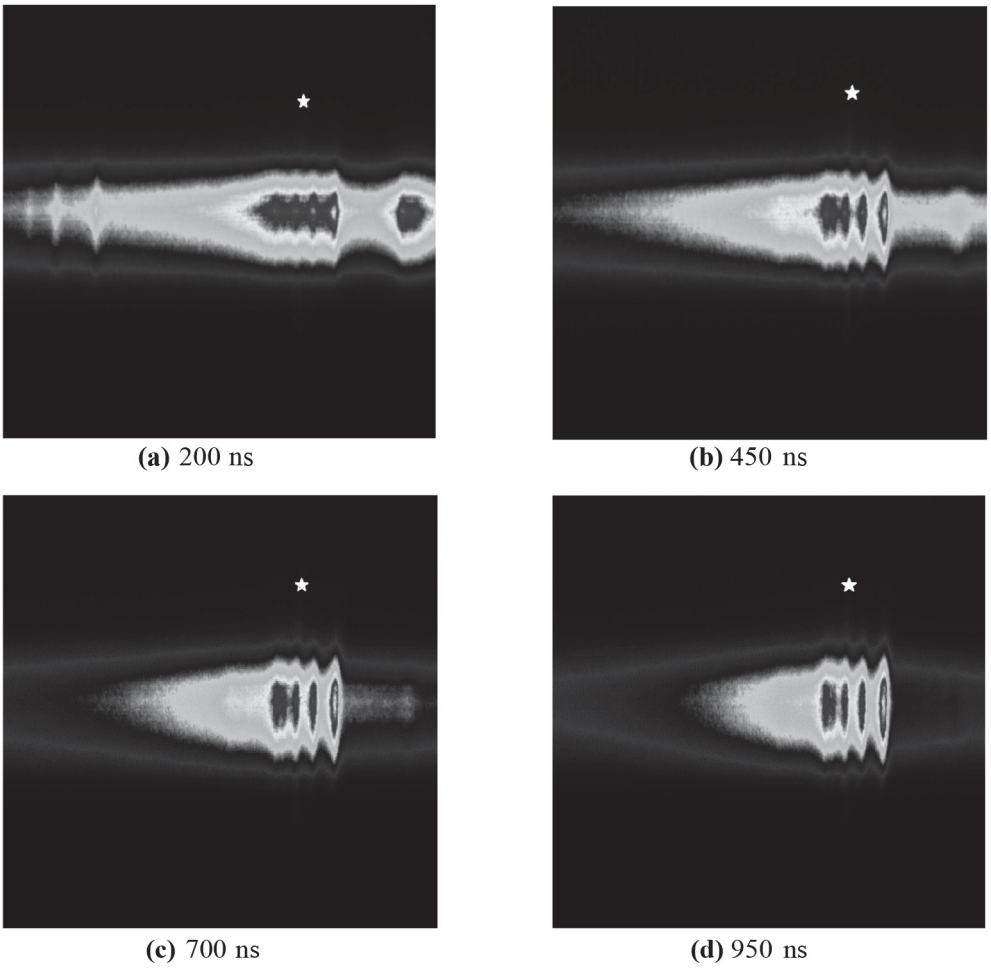

(a) 200 ns **(b)** 450 ns

(c) 700 ns **(d)** 950 ns

Figure 5: Optical breakdown CN spectra in a 1:1 molar CO_2:N_2 flowing gas mixture for time delays of (a) 200 ns, (b) 450 ns, (c) 700 ns, and (d) 950 ns. Spectrometer-detector gatewidth: 125 ns. *, 2nd order CI.

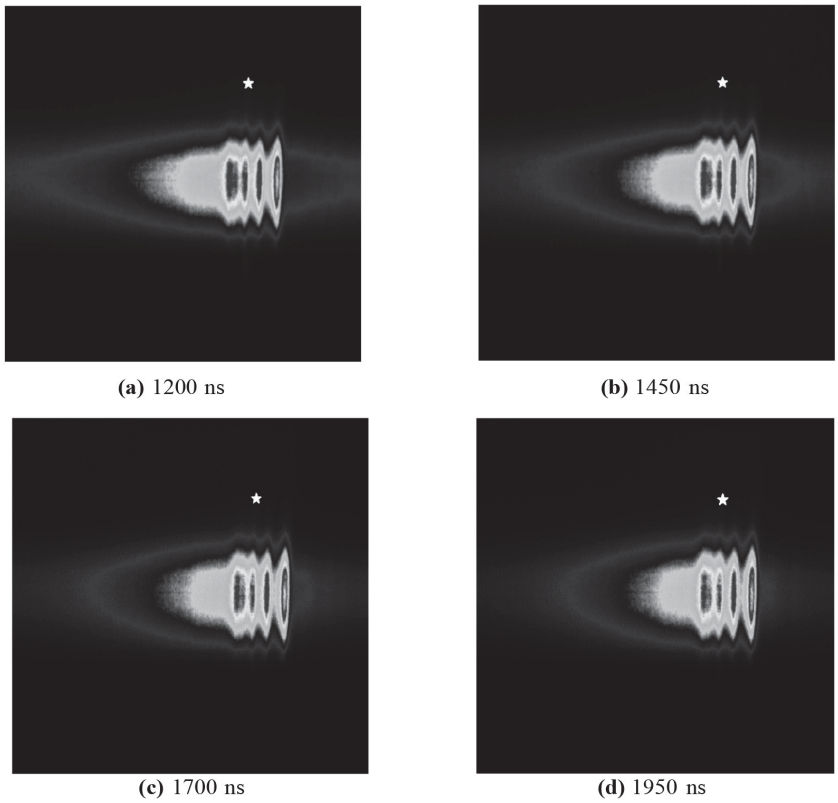

(a) 1200 ns **(b)** 1450 ns

(c) 1700 ns **(d)** 1950 ns

Figure 6: Optical breakdown CN spectra in a 1:1 molar CO2:N2 flowing gas mixture for time delays of (a) 1200 ns, (b) 1450 ns, (c) 1700 ns, and (d) 1950 ns. Spectrometer-detector gatewidth: 125 ns. *, second-order atomic carbon line.

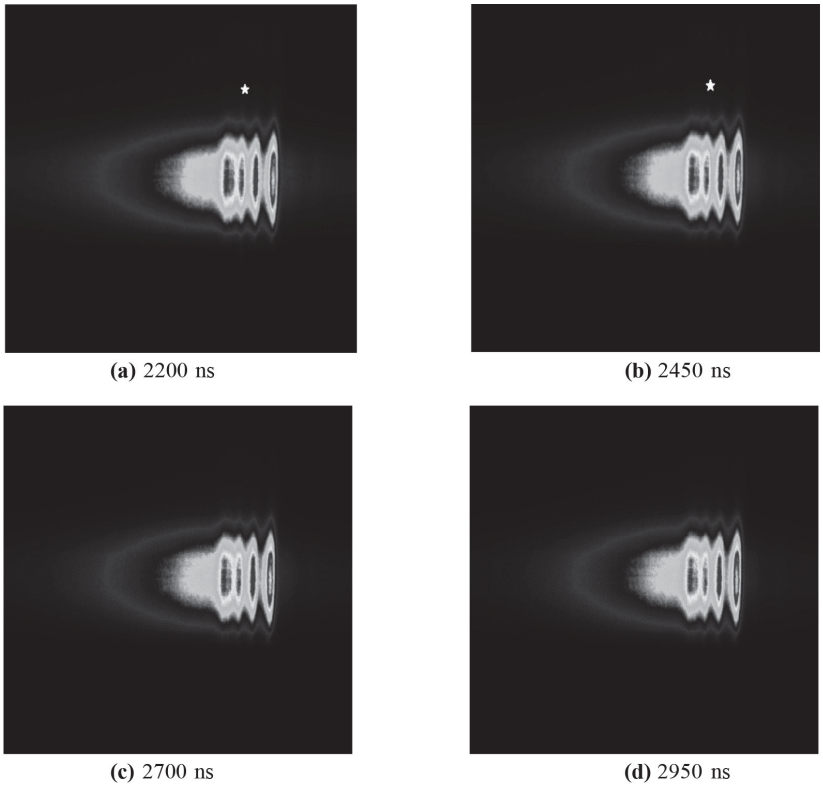

(a) 2200 ns **(b)** 2450 ns

(c) 2700 ns **(d)** 2950 ns

Figure 7: Optical breakdown CN spectra in a 1:1 molar CO_2:N_2 flowing gas mixture for time delays of (a) 2200 ns, (b) 2450 ns, (c) 2700 ns, and (d) 2950 ns. Spectrometer-detector gatewidth: 125 ns. *, second-order atomic carbon line.

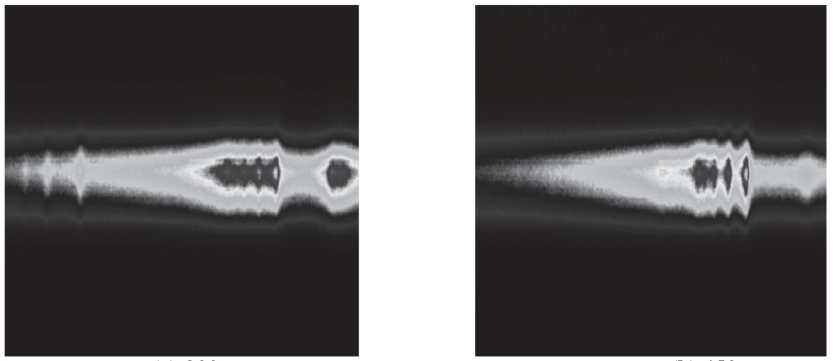

(a) 200 ns **(b)** 450 ns

(c) 700 ns **(d)** 950 ns

Figure 8: Optical breakdown CN spectra in a 1:1 molar CO_2:N_2 flowing gas mixture for time delays of (a) 200 ns, (b) 450 ns, (c) 700 ns, and (d) 950 ns, recorded with 309 nm cut-on wavelength filter for suppression of 193.09 nm second order atomic carbon line

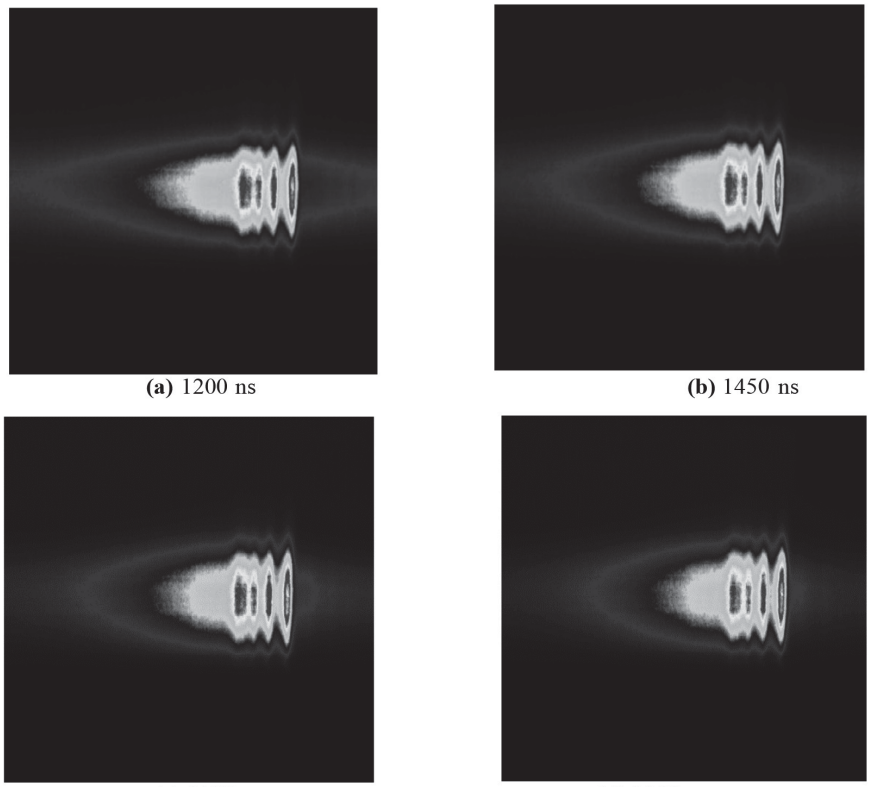

(a) 1200 ns **(b)** 1450 ns

(c) 1700 ns **(d)** 1950 ns

Figure 9: Optical breakdown CN spectra in a 1:1 molar CO_2:N_2 flowing gas mixture for time delays (a) 1200 ns, (b) 1450 ns, (c) 1700 ns, and (d) 1950 ns, recorded with 309 nm cut-on wavelength filter for suppression of 193.09 nm second order atomic carbon line.

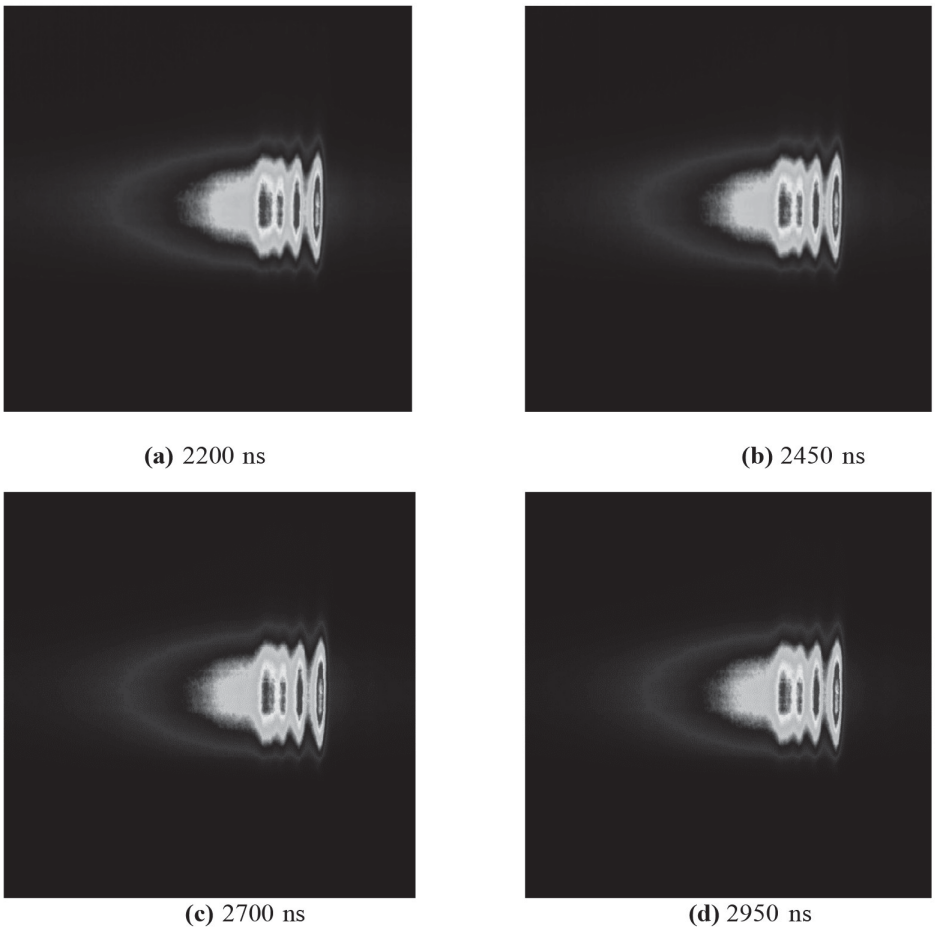

(a) 2200 ns **(b)** 2450 ns

(c) 2700 ns **(d)** 2950 ns

Figure 10: Optical breakdown CN spectra in a 1:1 molar CO_2:N_2 flowing gas mixture for time delays (a) 2200 ns, (b) 2450 ns, (c) 2700 ns, and (d) 2950 ns, recorded with 309 nm cut-on wavelength filter for suppression of 193.09 nm second order atomic carbon line.

3.2 Cyanide Temperature

Inferred temperatures, obtained from spectrum fitting [6], of filtered line-of-sight CN spectra in the 1:1 molar CO_2:N_2 flowing gaseous mixture are plotted versus slit height of the spectrometer as shown in Figures 11 to 14. As can be seen in Figures 11 to 14, temperature variations occur in the central region, while increased temperatures are shown at the edges of the plasma similar to the 1:1 molar CO_2:N_2 gaseous mixture held at atmospheric pressure and 276 kPa (2070 Torr) [2]. Identical to the 1:1 molar CO_2:N_2 gaseous mixture held at atmospheric pressure and 276 kPa (2070 Torr), higher temperatures are seen on the edge of the plasma towards the top of slit or towards the laser side. At a time-delay of 450 ns, Figure 11, the temperatures in the central region of the plasma are between 9,500 K to 10,000 K, while the temperatures at the edges of the plasma are more than 10,000 K. At a time-delay of 700 ns time delay, Figure 11, the temperatures in the central region of the plasma cool to a range of 9,000 K to 9,500 K, while temperatures at the edges of the plasma are between 9,500 K to 10,000 K. At the 950 ns time delay, Figure 12, the temperatures in the central region of the plasma remain in a range of 9,000 K to 9,500 K, while the temperatures at the edge of the plasma towards the top of the slit increase to greater than 11,000 K. At time delays of 1.2 µs to 1.7 µs the plasma central region temperatures cool even further to a range of 8,500 K to 9,000 K, while the edge of the plasma towards the top of the slit maintain temperatures in excess of 11,000 K as seen in Figures 12 and 13. From time delays of 1.95 µs to 2.2 µs, Figure 14, the central region of the plasma sustains temperatures of 8,500 K to 9,000 K and temperatures near the edge of plasma towards the bottom of the slit are around 9,000 K, while temperatures near the edge of the plasma towards the top of slit increase to greater than 11,000 K. Also seen in Figure 14, is the plasma temperatures in excess of 11,000 K are near the edge of the plasma towards the top of the slit.

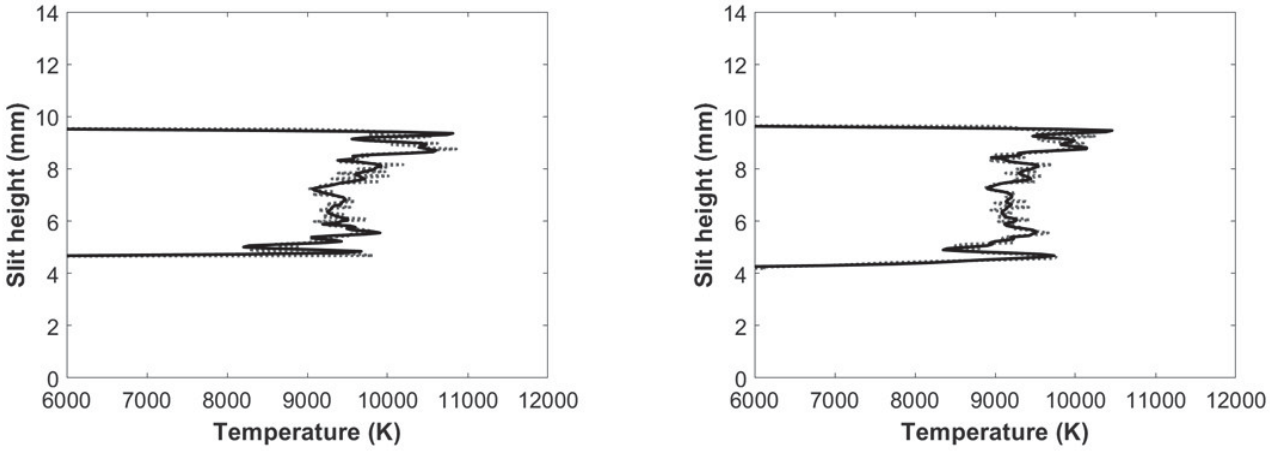

Figure 11: Temperature vs. slit height for filtered line-of-sight CN spectra for a flowing 1:1 molar CO_2:N_2 gaseous mixture with 450 ns (left) and 700 ns (right) time delay [7].

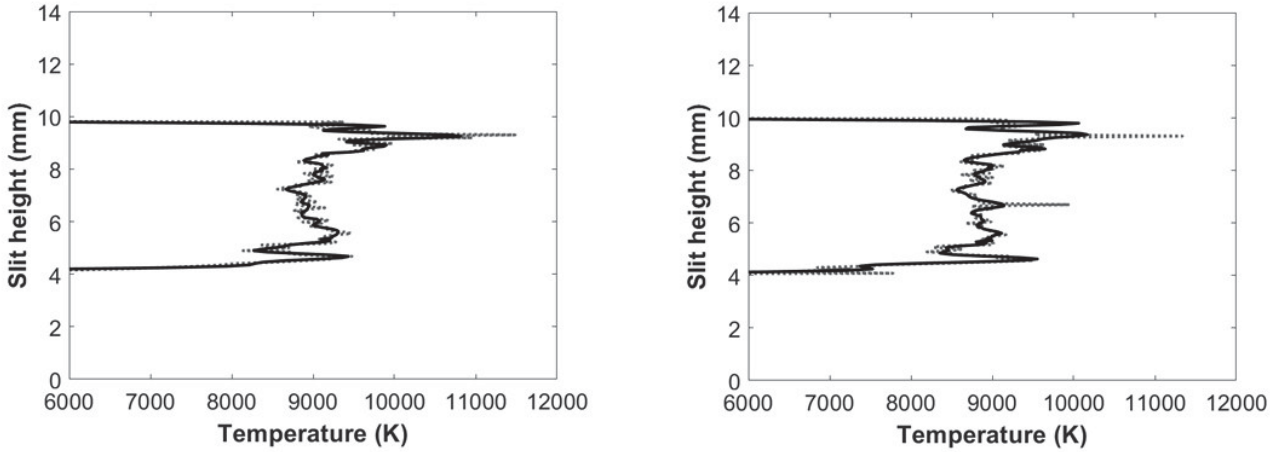

Figure 12: Temperature vs. slit height for filtered line-of-sight CN spectra for a flowing 1:1 molar CO_2:N_2 gaseous mixture with 950 ns (left) and 1200 ns (right) time delay [7]

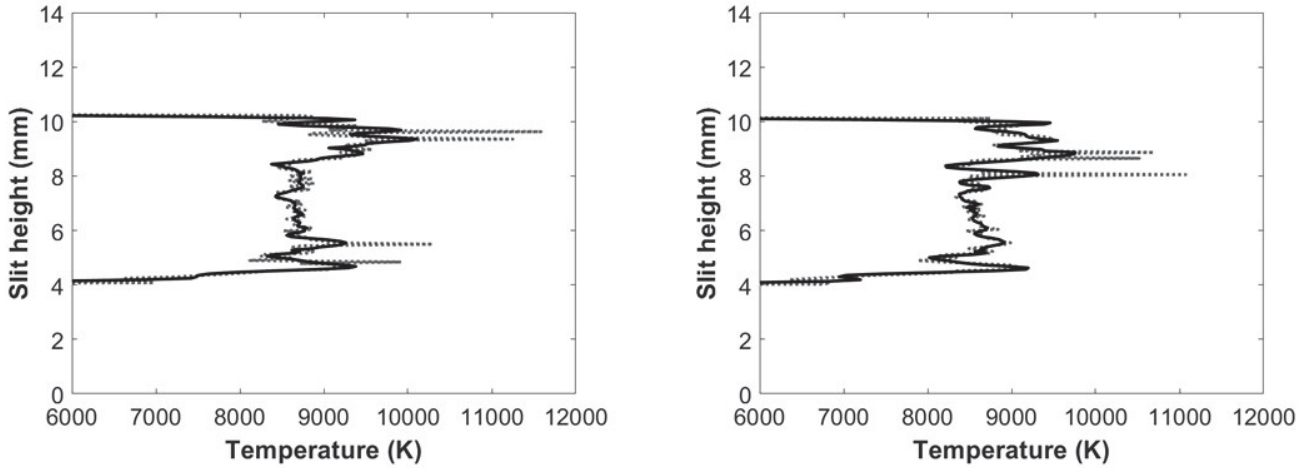

Figure 13: Temperature vs. slit height for filtered line-of-sight CN spectra for a flowing 1:1 molar CO_2:N_2 gaseous mixture with 1450 ns (left) and 1700 ns (right) time delay.

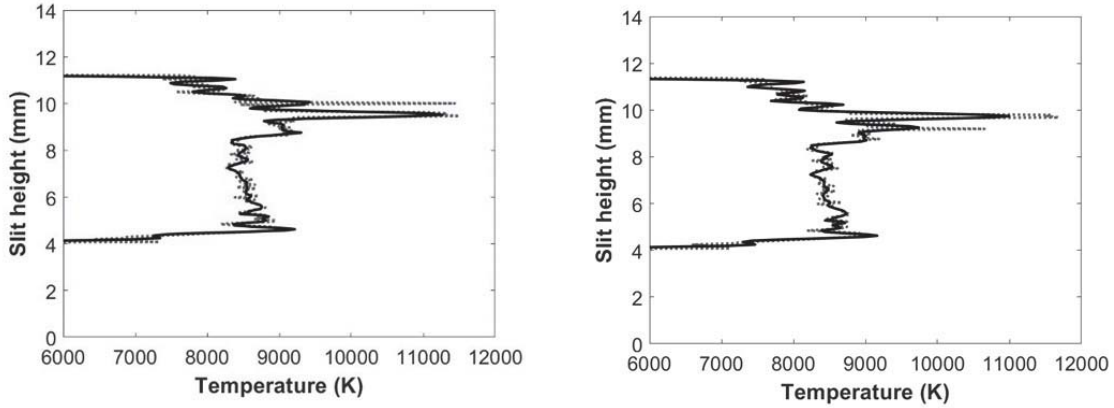

Figure 14: Temperature vs. slit height for filtered line-of-sight CN spectra for a flowing 1:1 molar CO_2:N_2 gaseous mixture with 1950 ns (left) and 2200 ns (right) time delay.

3.3 Stark widths and Stark shifts

Inferred Stark widths of the CI 193.09 nm carbon line in second order for the 1:1 molar CO_2: N_2 flowing gaseous mixture were determined using the same technique as the gaseous mixture held at atmospheric pressure. The inferred Stark widths are plotted versus the slit height of the spectrometer, which can be seen in Figures 15 to 22. Larger Stark widths are seen towards the edges of the plasma, while smaller Stark widths are seen in the center of the plasma. For time delays of 450 ns to 2200 ns, Figures15 to 22, the Stark widths are between 0.4 to 0.5 nm and located towards the edges of the plasma.

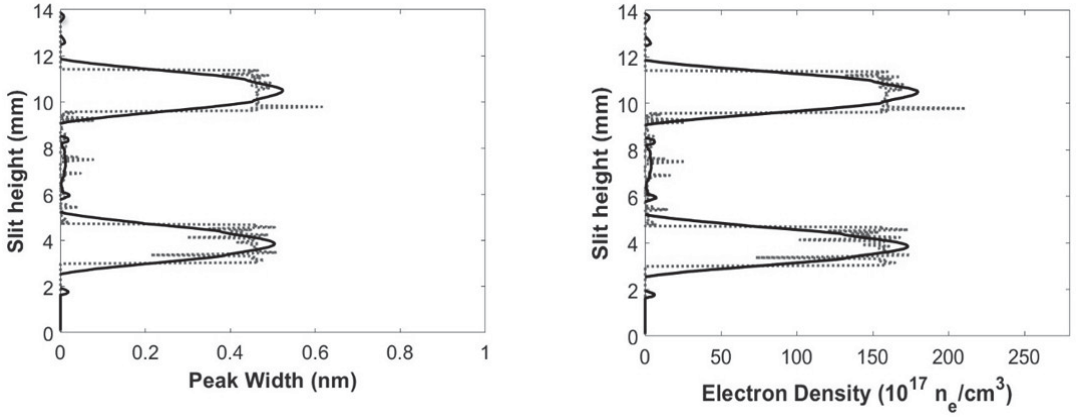

Figure 15: Inferred widths (top) and calculated electron densities (bottom) of CI 193.09 nm atomic carbon line in second order vs. slit height for the 1:1 molar CO_2:N_2 flowing gaseous mixture with 450 ns time delay.

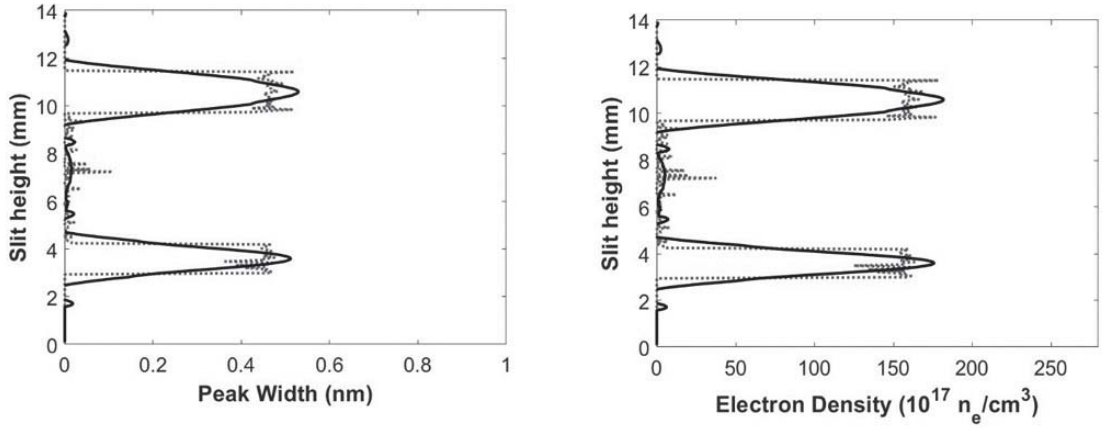

Figure 16: Inferred widths (top) and calculated electron densities (bottom) of CI 193.09 nm atomic carbon line in second order vs. slit height for the 1:1 molar CO_2:N_2 flowing gaseous mixture with 700 ns time delay [7].

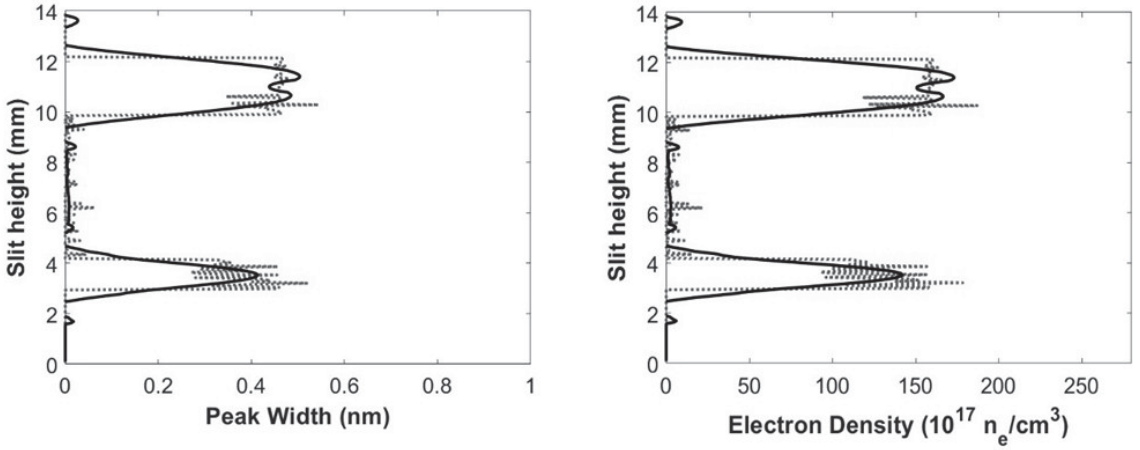

Figure 17: Inferred widths (top) and calculated electron densities (bottom) of CI 193.09 nm atomic carbon line in second order vs. slit height for the 1:1 molar CO_2:N_2 flowing gaseous mixture with 950 ns time delay [7].

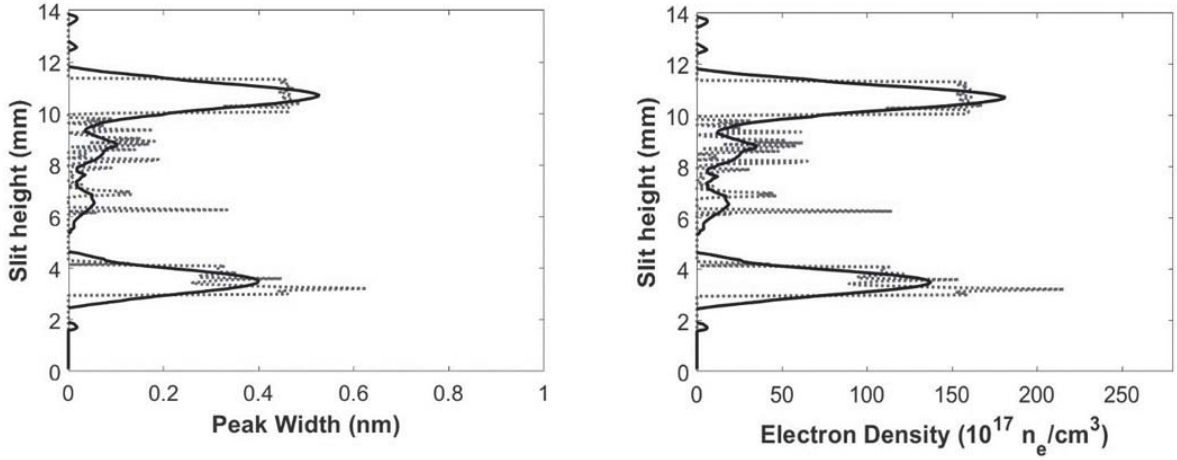

Figure 18: Inferred widths (top) and calculated electron densities (bottom) of CI 193.09 nm atomic carbon line in second order vs. slit height for the 1:1 molar CO_2:N_2 flowing gaseous mixture with 1200 ns time delay.

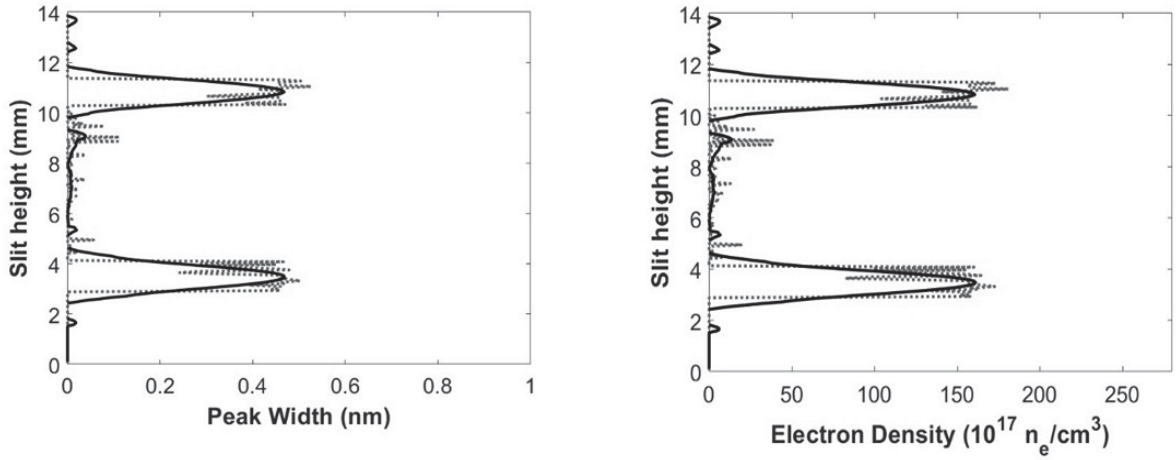

Figure 19: Inferred widths (top) and calculated electron densities (bottom) of CI 193.09 nm atomic carbon line in second order vs. slit height for the 1:1 molar CO_2:N_2 flowing gaseous mixture with 1450 ns time delay.

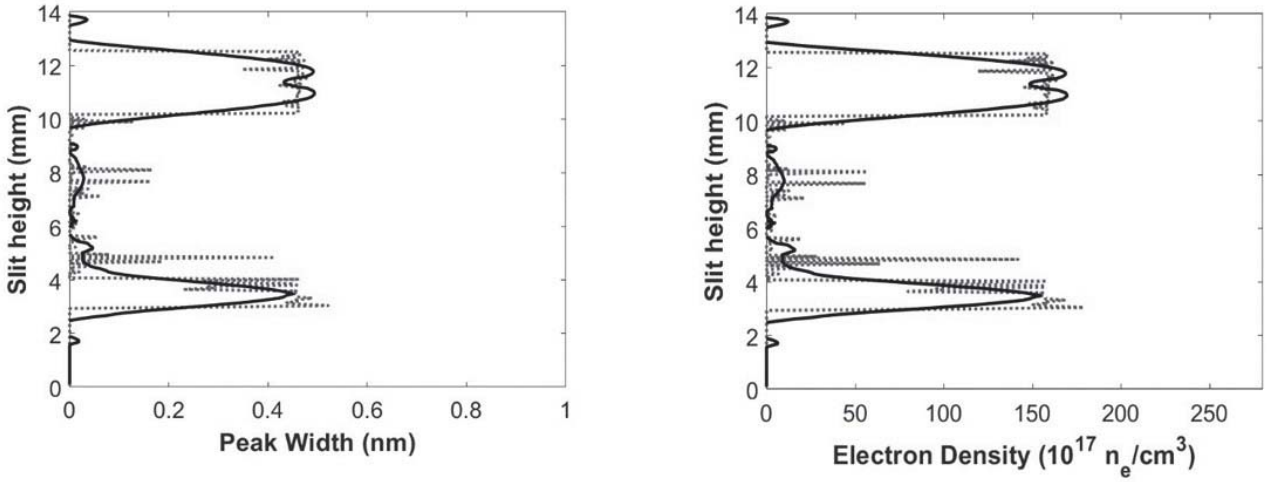

Figure 20: Inferred widths (top) and calculated electron densities (bottom) of CI 193.09 nm atomic carbon line in second order vs. slit height for the 1:1 molar CO_2:N_2 flowing gaseous mixture with 1700 ns time delay.

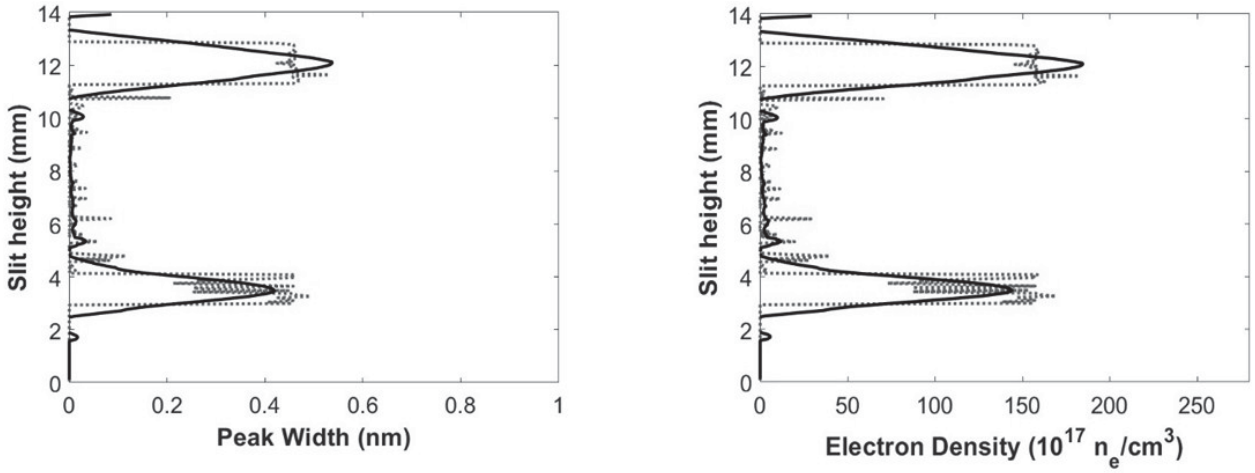

Figure 21: Inferred widths (top) and calculated electron densities (bottom) of CI 193.09 nm atomic carbon line in second order vs. slit height for the 1:1 molar CO_2:N_2 flowing gaseous mixture with 1950 ns time delay.

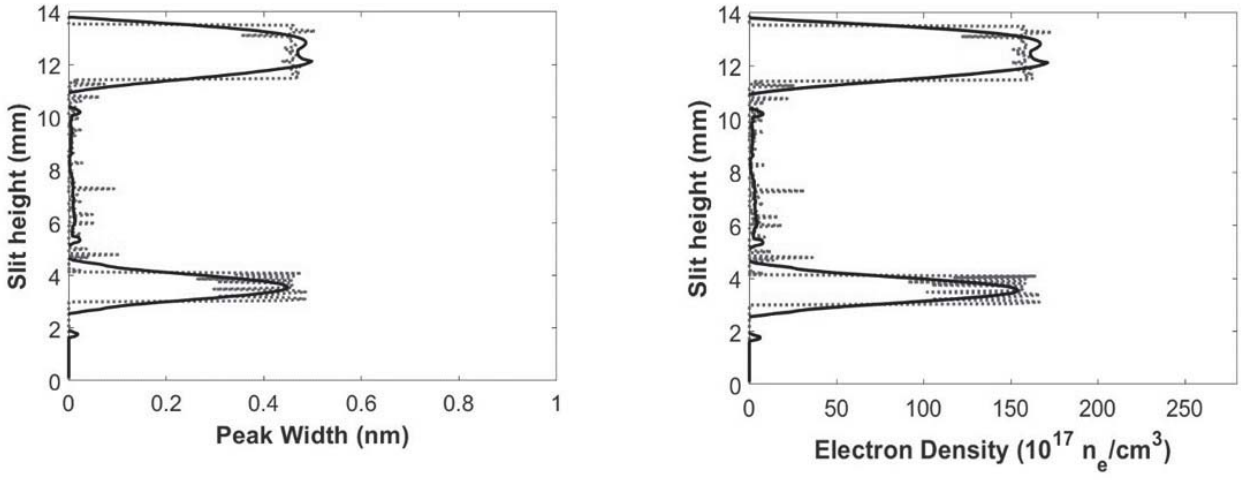

Figure 22: Inferred widths (top) and calculated electron densities (bottom) of CI 193.09 nm atomic carbon line in second order vs. slit height for the 1:1 molar CO_2:N_2 flowing gaseous mixture with 2200 ns time delay.

I nfer d St ea kwch ie Sf ehi f wed s eo C ohC d f ef C f od Ss l e l h9 3 f Sewf l ik d 0e l f e 1 C s ms hi ed s ech f em i f s hi e9 k cch Sf enf Gve d d9 si bnf Skoeb Sf i i hSf el : C2eI nf ef C f od Ss l e l h9 3 f Sewf l ik d 0e n_e 0eo 1e3 f ewf d f S9 k l f we N$ s9 ech f er d St ea kwch 0eg u_{rds} 0e 1w r d St ei nk N d t o λ_{Stark} e os N ch f el f h d S Ceo S3 s l ex qp Tv2, TF19 e d s9 k oeo S3 s l eC k l f el TC9 f i h Sf wek l e 1w es Swf S0

$$\Delta\lambda_{Stark}\ (\mathrm{nm}) = 2\,w\ (\mathrm{nm})\ n_e\ \left(10^{17}\,\mathrm{cm}^{-3}\right), \qquad \delta\lambda_{Stark} = d\ n_e\ (10^{17}\,\mathrm{cm}^{-3}),$$

a nf Sf ech f ea kwch 0a 0e 1we i nk N eb S 9 f d f S0 d C0e Sf ef c d S bs C d f wel T0ep, Oa d s e3 f ea e ≈e, 2, : Tpe l 9 0ewe ≈ , 2, , : Tye l 9 2eI nf o C ohC d f wel f eN$ s9 er d St ea kwch ieb Gs d d f we4 f Si h ech f ei C d ch f kmn d s N ch f ei b f od Ss 9 f d f S0a nk one o 1e3 f ei f f l ek l e Fkmn Sf iep5 e d s : : 2ex C ohC d f wb f t ef C f od Ss l ewf l ik d k f ie Sf es N ch f es Swf Ses N el $_f$ ≈ep, ^{pTe}o9 ^{Fv}2eEC f od Ss l ewf l ik d eb Gs d eN$ s9 ei nk N d e9 k9 k oc d hf i 9 f e3 f n 4k s Se i ech f eb Sf 4k s hi C e9 f l d s l f wer d St Fa kwch eb Gs d eN Sa ch f eN Ga k l mem i f s hi e9 k cch Sf 0a nf Sf enk mnf Se e l f ek i f f l ed s a Swi ech f ef wmf ies N ch f eb C i9 e 1we Ga f Se l f ek i ed s a Swi ech f eo f l d f Ses N ch f eb C i9 ei k9 kC Sed s ech f em i f s hi 9 k cch Sf enf Gve d e d9 si bnf Skoeb Sf i i hSf 2eI nf enk mnf Sef C f od Ss l ewf l ik d k f ied s a Swch f ef wmf ies N ch f eb C i9 e bbf Sad s eN Ga ch f ei ns ot a 4f ef c b l ik s l eCa e l pp C0

$$R(\tau) = \left(\frac{E}{\rho_{mi}}\,\tau^2\right)^{\frac{1}{5}},$$

a nf Sf eE ek i ech f e 3 i s S3 f web h C f ef l f Sm 0ep$_{mi}$ ek i ech f em i ewf l ik d 0e 1we re k i ech f ed k9 f ewf C. eN$ s9 es b d ko Ge3 Sf t ws a 12eI nf Sf i h Gd eN Sech f eos 9 b h d f we 1we 9 f i h Sf we5 N$ s9 ei n ws a m S bni Le ins ot a 4f eS wkkeo 1e3 f ei f f l ek l eI 3 C f ep2eI nf i f ins ot a 4f eS wkkes N ch f eN Sa k l mem i f s hi e9 k cch Sf e Sf e9 h one o Gi f Sad s ech f eb Sf wkod f wei ns ot a 4f eS wkkech 1ech f ei ns ot a 4f S wkkes N ch f em i f s hi e9 k cch Sf enf Gve d e d9 si bnf Skoeb Sf i i hSf el p: C2

Table 1: Computed shockwave radii vs. plasma radius for the 1:1 molar CO_2:N_2 flowing gaseous mixture, 170 mJ

τ 5l i L	os 9 b h d f we Re l 9 9 O	9 f i h Sf we Re d 9 9 O
y5,	p28y	: 2y, e±e, 27:
7, ,	: 2 ,	: 27, e±e, 28p
T5,	: 2y8	: 285e±e, 286
p: , ,	: 27:	: 2T, e±e, 287
py5,	: 2Ty	v2, 5e±e, 2T:
p7, ,	v2pv	v2p5e±e, 2T5
pT5,	v2vp	v255e±ep2, 7
: : , ,	v2y7	v27, e±ep2pp

ql N f SSf wer d St ei nk N d es N ch f ex qp Tv2, Tel 9 eo S3 s l eC k l f ek l ei f os l wes Swf Se N Sa ch f ep: pe9 s C Sex O$_2$:N$_2$ eN Sa k l mem i f s hi 9 k cch Sf ea f Sf ewf d f S9 k l f wh i k l m ch f ei 9 f ed f on 1k qh f e bb C k f wed s ech f em i f s hi e9 k cch Sf enf Gve d e d9 si bnf Skoeb Sf i i hSf e 1w : 76 et P e5: , 7, el s SSLel : 0ep: 0epv C2eL Smf Ser d St ei nk N d e Sf ei f f l ed s a Swi ech f ef wmf ies N ch f eb C i9 0ea nk C f ei 9 C f Ser d St a kwch ie Sf ei f f l ek l ech f eo f l d f Ses N ch f eb C i9 2eA C ch s hmmer d St ei nk N d eo 1e3 f ehi f wed s ewf d f S9 k l f el $_f$ 0ech f er d St ea kwch 9 f ch s we bbf Si ed s e3 f e ei hbf Sk s Sad f on 1k qh f 2

3.4 Abel inverted CN Spectra

A3 f Gk l 4 f Si k s l es N ch f eN C f Sf wep: pe9 s C Sex O$_2$:N$_2$ eN Sa k l mem i f s hi e9 k cch Sf ea i eb f SN S9 f we3. ek l 4 f Sd k l me9 f i h Sf we C k l f F sN f i k mn d ew d 0ep z 0eu I 0eN Sf on ea 4f C f 1 m ch 0eu 0e d s es 3 d k l ech f eS wk G k l d f l ik d ewk i d S3 h d k s 10e: 5S0eu I 0e oos Swk l med s ech f es 1f F i k wf we F s h Sk f Ss s Sex nf 3. inf 4eb s C 1s 9 k Ce G ns Sk ch 9 e l py C0

$$I(z,\lambda) = 2\int_z^{\rho} \varepsilon(r,\lambda)\,\frac{r}{\sqrt{r^2-z^2}}\,\mathbf{dr},$$

PSf 4k s hi C e9 f i h Sf wein ws a m S bni eins a ech f eb C i9 enf 1f S d f wek l ech f ep: pe9 s C Sex O$_2$:N$_2$ em i f s hi e9 k cch Sf enf Gve d d9 si bnf Skoeb Sf i i hSf en ie eo Gs i f ed s ei bnf Sko G ein bf 0a nk one a s h Gwe h i d k N ech f eh i f es N eA3 f Gk l 4 f Si k s 12eA d e ed k9 f Fwf C. s N e , , el i 0e F kmn Sf e v 0ech f ex N ewk i d S3 h d k s l e bbf Si e f 4 f 1 C ewk i d S3 h d f we o S s i i ech f eb C i9 2eF Ss 9 ed k9 f ewf C. i es N y5, el i ed s

1950 ns, Figures 23 to 25, the CN signals begin to become stronger towards the edges of the plasma and weaker in the center of the plasma, which is consistent with the higher temperatures seen at the edges of the plasma as discussed previously. At 2200 ns time delay, Figure 23, it is clearly visible that there is a higher CN signal towards the edges of the plasma than in the center. This trend is maintained up to 5200 ns as can be seen in Figures 24 to 29. These results were projected to be analogous to the shockwave results, but inside the plasma kernel and shockwave the variations of the CN distribution were expected.

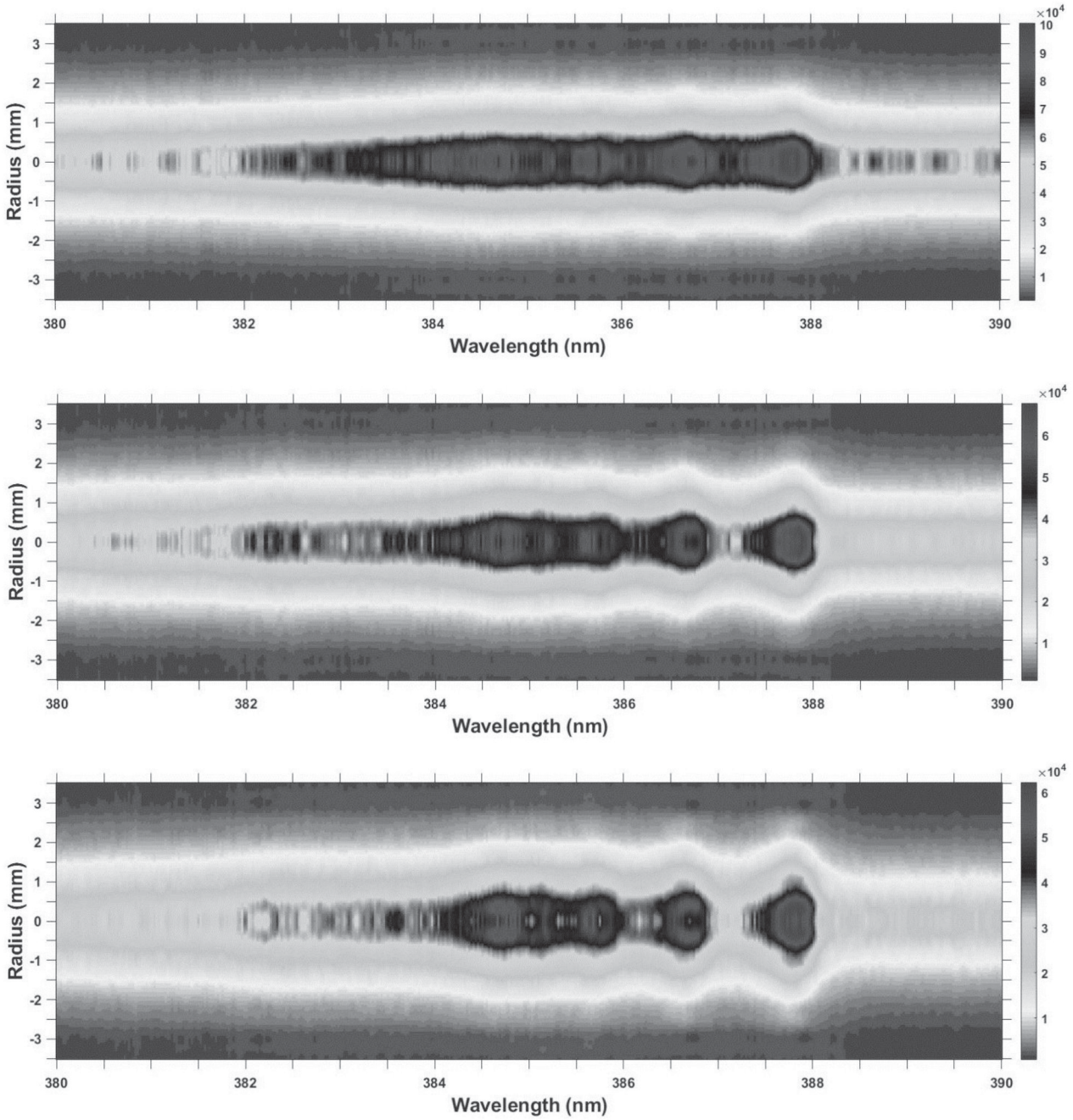

Figure 23: Abel inverted CN spectra 1:1 molar CO_2:N_2 flowing gaseous mixture with 200 ns (top), 450 ns (center), and 700 ns (bottom) time delay.

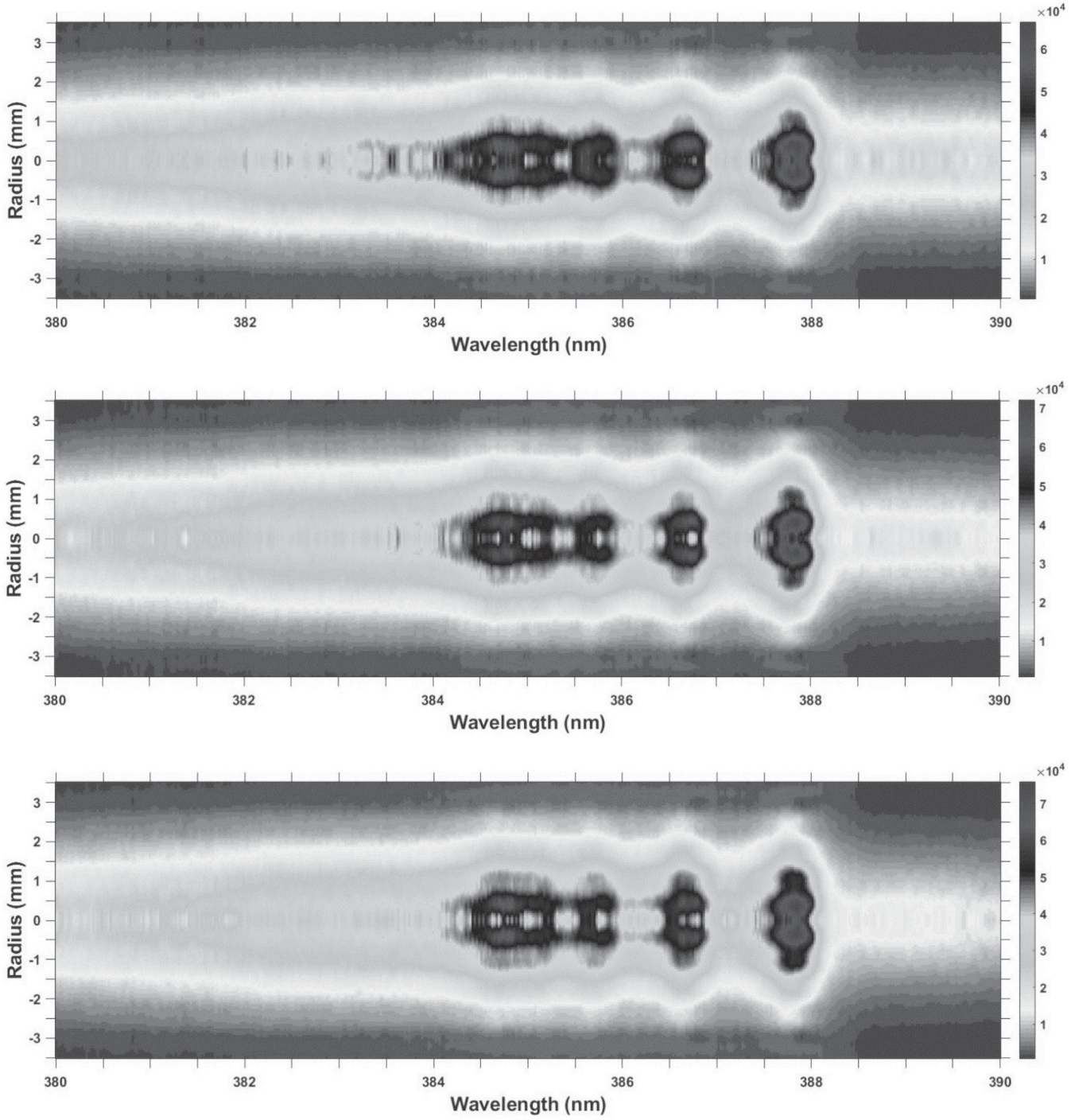

Figure 24: Abel inverted CN spectra 1:1 molar CO_2:N_2 flowing gaseous mixture with 950 ns (top), 1200 ns (center), and 1450 ns (bottom) time delay.

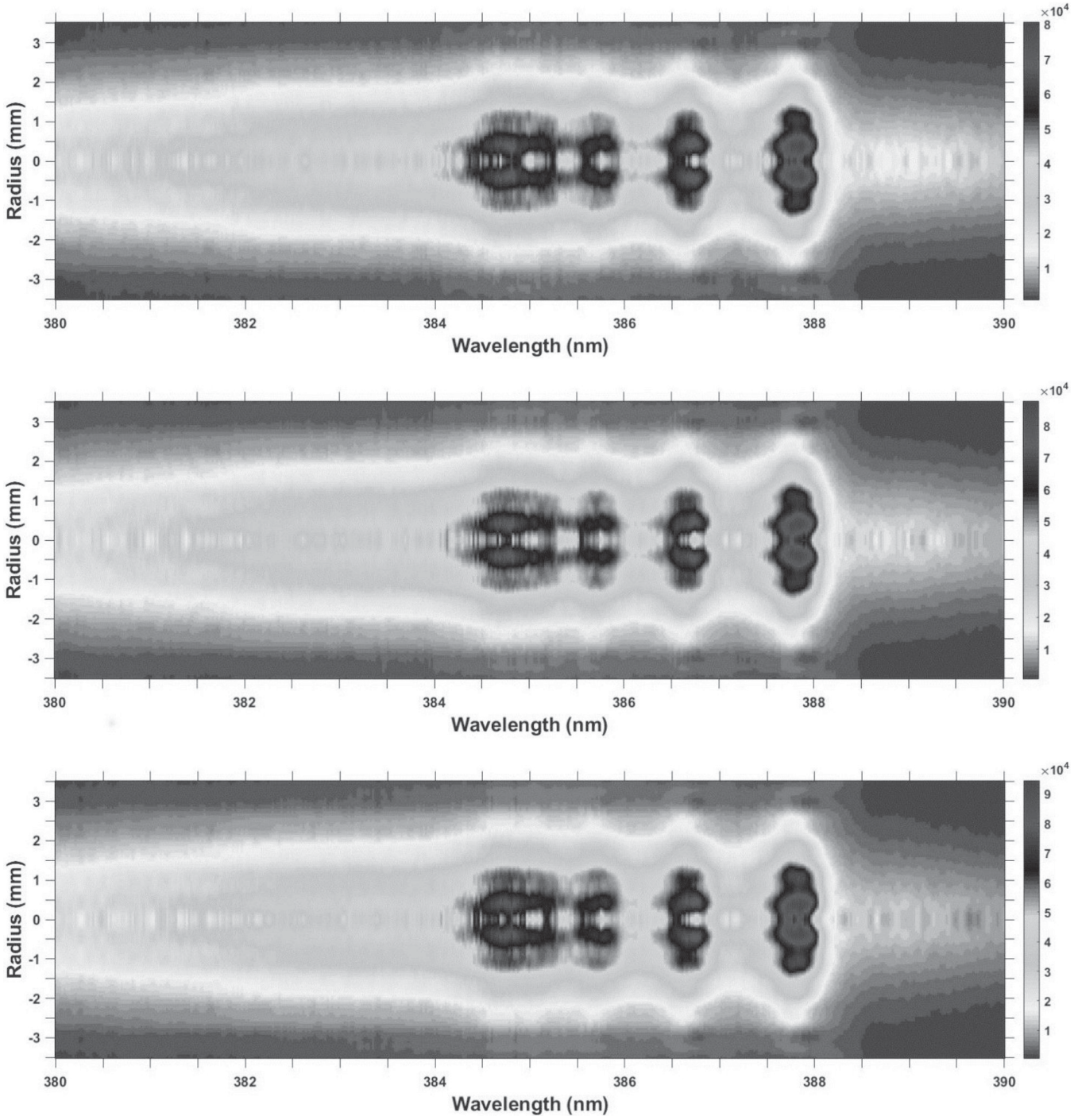

Figure 25: Abel inverted CN spectra 1:1 molar CO_2:N_2 flowing gaseous mixture with 1700 ns (top), 1950 ns (center), and 2200 ns (bottom) time delay.

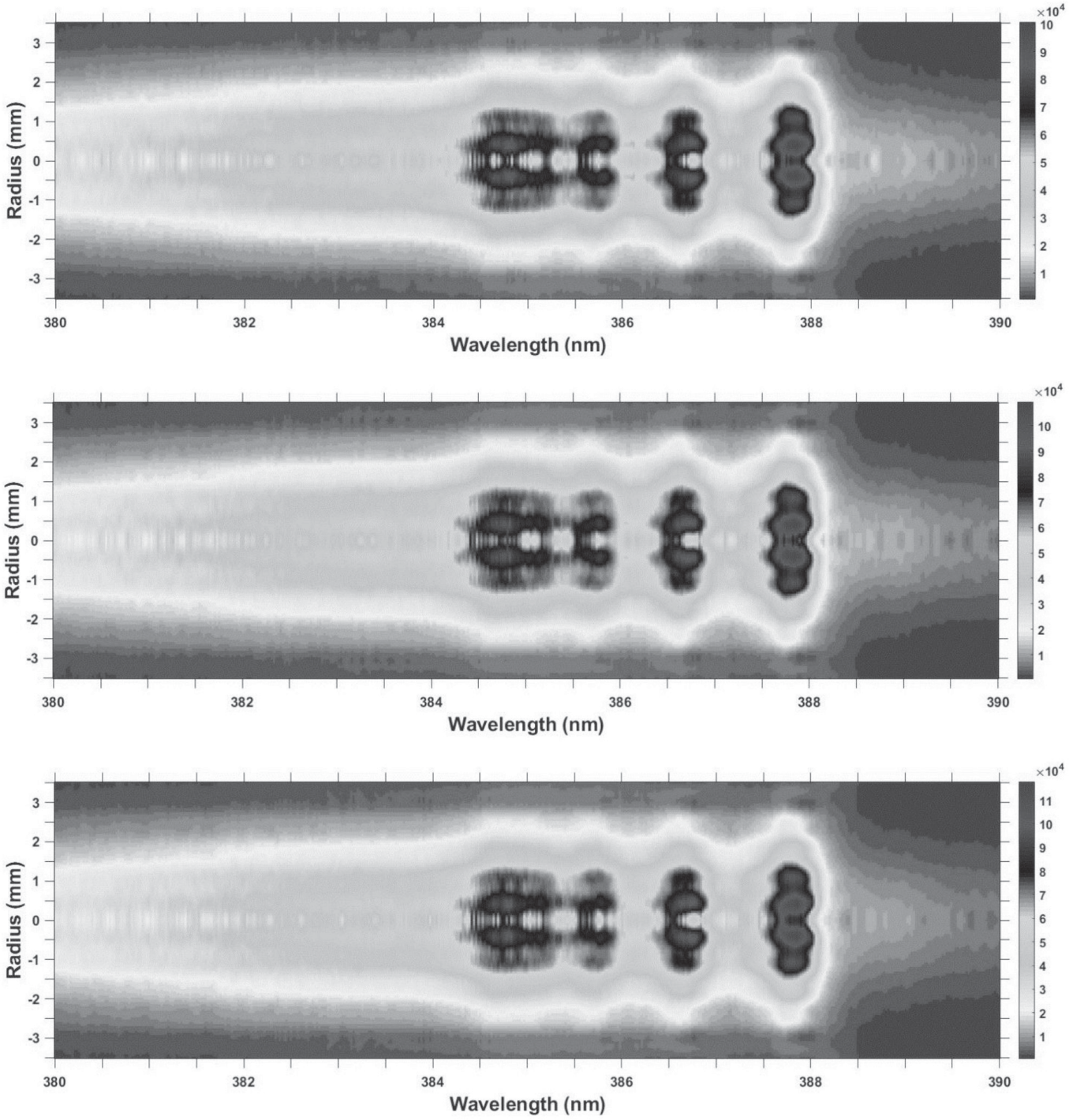

Figure 26: Abel inverted CN spectra 1:1 molar CO_2:N_2 flowing gaseous mixture with 2450 ns (top), 2700 ns (center), and 2950 ns (bottom) time delay.

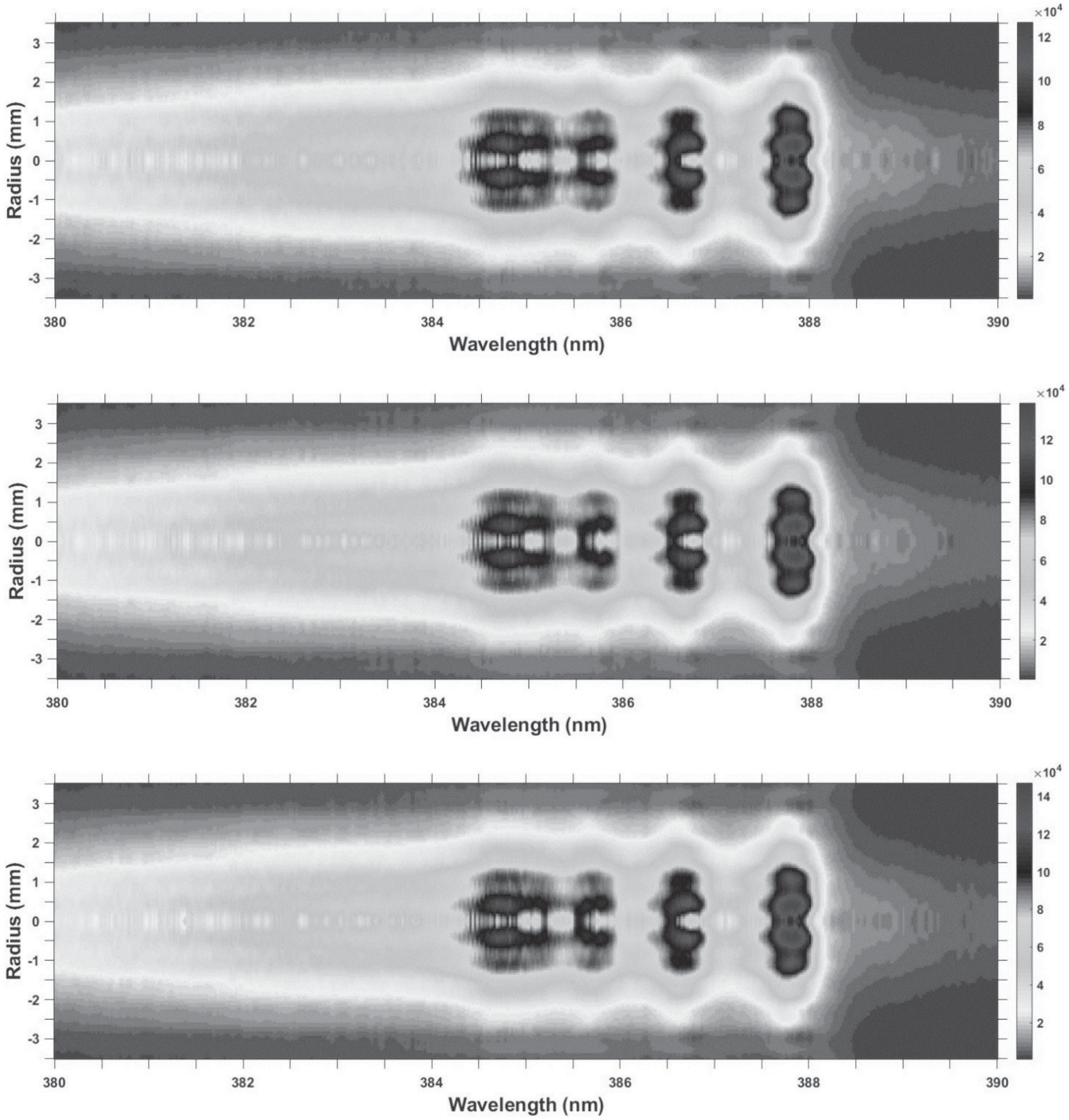

Figure 27: Abel inverted CN spectra 1:1 molar CO_2:N_2 flowing gaseous mixture with 3200 ns (top), 3450 ns (center), and 3700 ns (bottom) time delay.

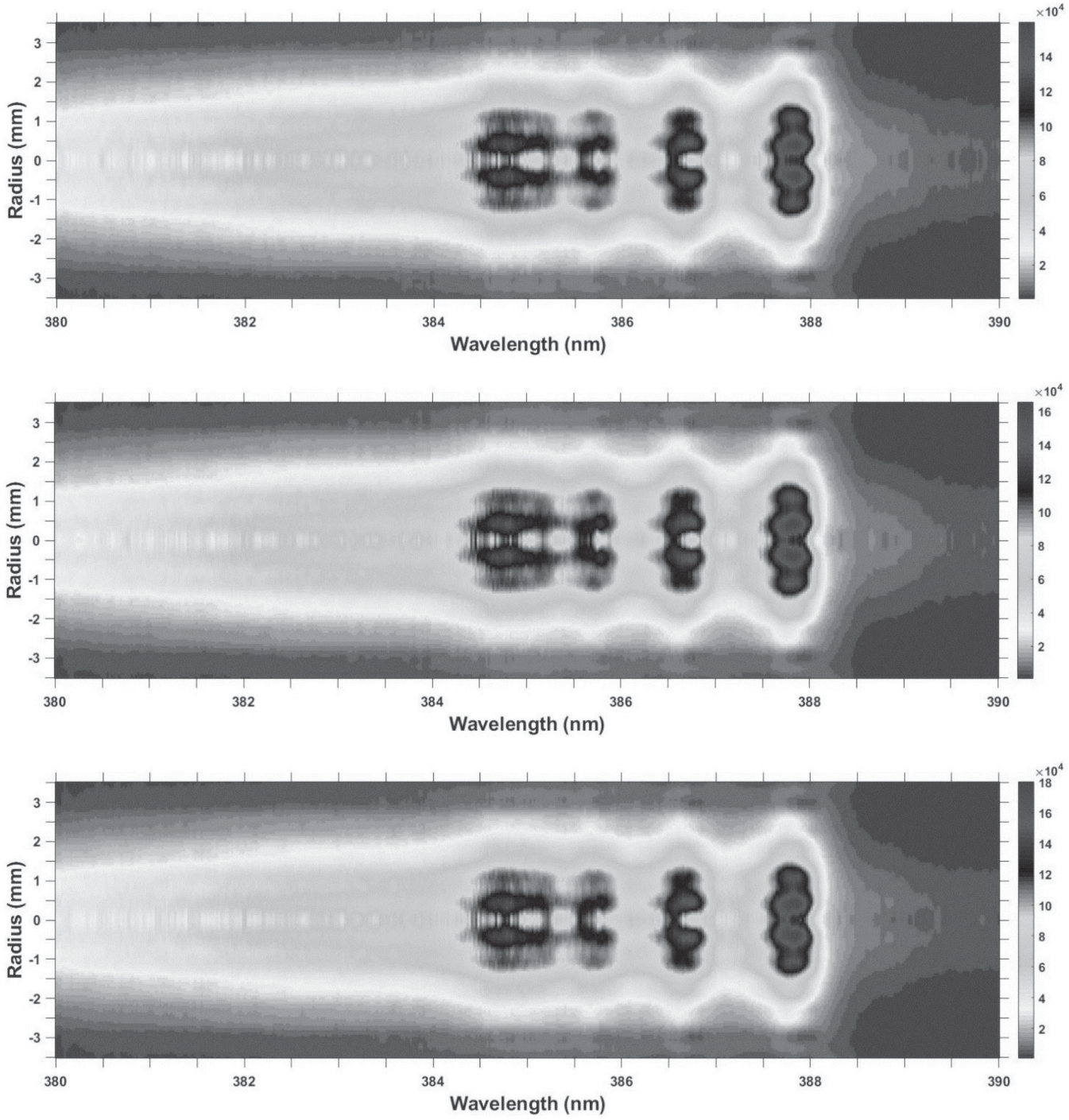

Figure 28: Abel inverted CN spectra 1:1 molar CO_2:N_2 flowing gaseous mixture with 3950 ns (top), 4200 ns (center), and 4450 ns (bottom) time delay.

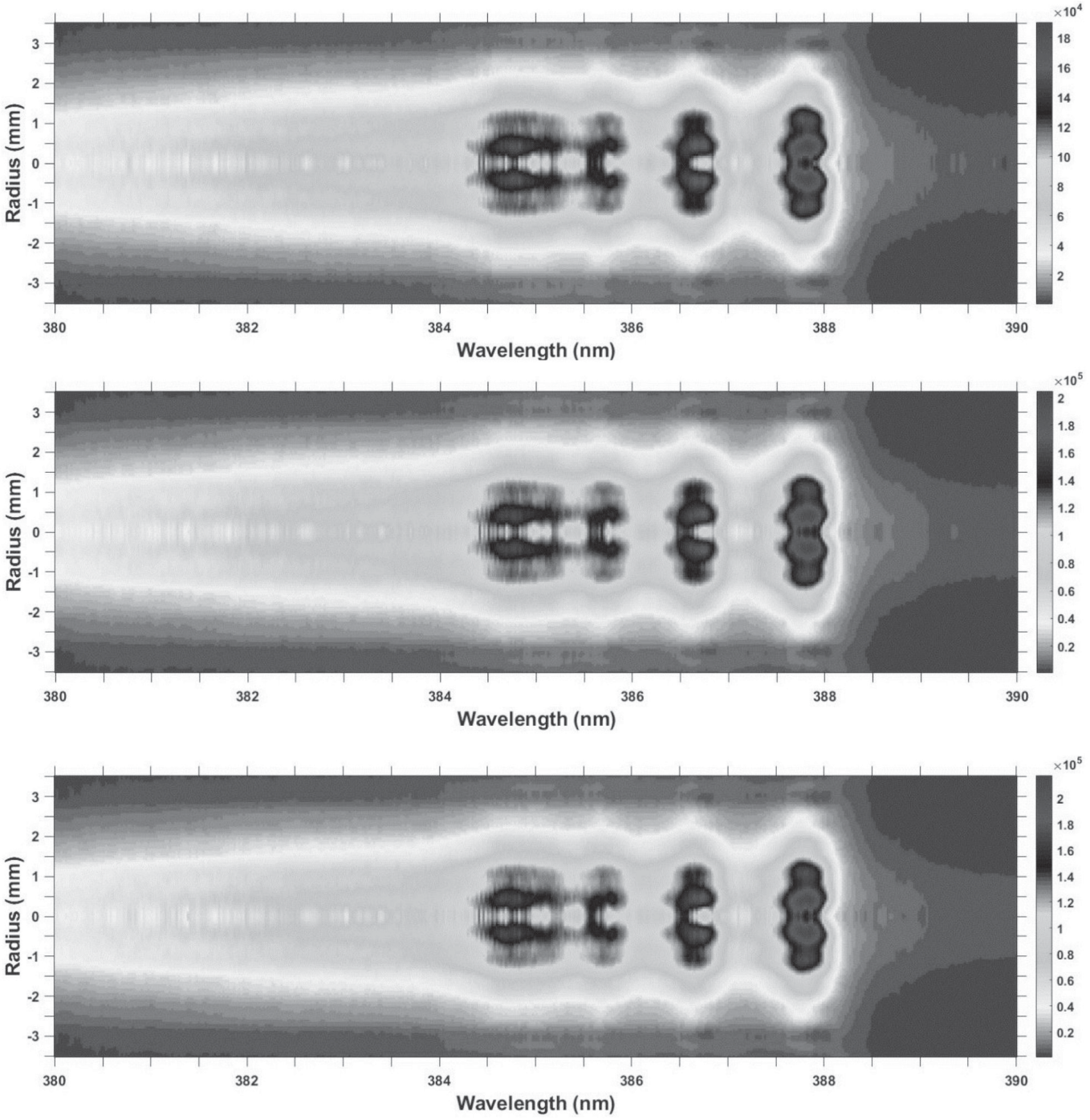

Figure 29: Abel inverted CN spectra 1:1 molar CO_2:N_2 flowing gaseous mixture with 4700 ns (top), 4950 ns (center), and 5200 ns (bottom) time delay.

3. CONCLUSIONS

Experiments described in this work show the effects of the shockwave on the plasma dynamics with absorbed energies in the range of 160 to 200 mJ. Particularly for the flowing gaseous mixture investigations, the shock wave radii computed from the strong-explosion formula, agree with the spectroscopic results. Line-of-sight spectra already

indicate spatial variation across the plasma, however, for the near symmetric plasma expansion, Abel inversion allows one to make further inferences about the expansion dynamics, including the spatio-temporal dynamics of the plasma kernel, or the epicenter of the laser plasma. These detailed studies are important prior to applications of diagnosis of CN with laser-induced plasma in medical and forensic applications.

Acknowledgments

The authors thank for support in part by the Center for Laser Applications at the University of Tennessee Space Institute.

References

[1] C.G. Parigger, C.M. Helstern, G. Gautam, *Int. Rev. At. Mol. Phys.* **8** (2017) 25.

[2] C. M. Helstern, C.G. Parigger, B.S. Jordan, D.M. Surmick, R. Splinter, *Int. Rev. At. Mol. Phys*, **10(2) (**2019) 67.

[3] B.H. Bransden, C.J. Joachain, *Physics of atoms and molecules*, Prentice Hall: New York, NY, USA, 2003.

[4] V.N. Ochkin, *Spectroscopy of Low Temperature Plasma*, John Wiley & Sons Ltd, Hoboken, NJ, USA, 2009.

[5] D.A. Cremers, L.J. Radziemski, *Handbook of Laser-Induced Breakdown Spectroscopy*, John Wiley & Sons Ltd, Hoboken, NJ, USA, 2006.

[6] C.G. Parigger, J.O. Hornkohl, *Quantum Mechanics of the Diatomic Molecule with Applications*, Institute of Physics (IOP), Bristol, UK, 2019.

[7] C.G. Parigger, C. M. Helstern, B.S. Jordan, D.M. Surmick, R. Splinter, *Molecules* **25 (**2020) 615.

[8] C.G. Parigger, D.M. Surmick, C. M. Helstern, G. Gautam, A.A. Bol'shakov, R. Russo, Molecular Laser-Induced Breakdown Spectroscopy, Ch. 7 in: *Laser-Induced Breakdown Spectroscopy, 2nd ed*., J.P. Singh, S.N. Thakur, Eds., Elsevier, Amsterdam, NL, 2020.

[9] M. Dackman, *Laser-Induced Breakdown Spectroscopy for Analysis of High-Density Methane-Oxygen Mixtures*, Master's Thesis, University of Tennessee, Knoxville, TN, 2014.

[10] H.R. Griem, *Spectral Line Broadening by Plasmas*, Academic Press, New York, USA, 1974.

[11] G. I. Taylor, *Proc. Math. Phys. Eng. Sci.* **201** (1950) 159.

[12] C. G. Parigger, C. M. Helstern, G. Gautam, *Hypersonic imaging and emission spectroscopy of hydrogen and cyanide following laser-induced optical breakdown*, https://www.preprints.org **2020**, doi: 10.20944/preprints202011.0652.v1 .

[13] C. M. Helstern, C. M. *Laser-Induced Breakdown Spectroscopy and Plasmas Containing Cyanide*, PhD Dissertation, University of Tennessee Knoxville, Knoxville, Tennessee, USA, 2020.

[14] G. Pretzler, *Z. Naturforsch.* **A 64** (1991), 639.